Journal of Colloid and Interface Science 678 (2025) 378–387

Contents lists available at ScienceDirect

Journal of Colloid And Interface Science

journal homepage: www.elsevier.com/locate/jcis

Regular Article

Responsive nanocellulose-PNIPAM millicapsules

Maryam Hosseini, Isaac J. Gresham, Stuart W. Prescott, Patrick T. Spicer *

School of Chemical Engineering, University of New South Wales, Sydney, NSW, Australia

GRAPHICAL ABSTRACT

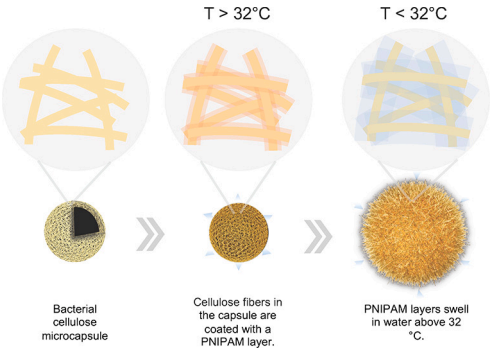

ARTICLE INFO

MSC:
2024
2000

Keywords:
Active matter
Nanocellulose
PNIPAM
Thermal responsive

ABSTRACT

Hypothesis: Milli- and micro-capsules are developed to facilitate the controlled release of diverse active ingredients by passive diffusion or a triggered burst. As applications expand, capsules are required to be increasingly multi-functional, combining benefits like encapsulation, response, release, and even movement. Balancing the increasingly complex demands of capsules is a desire to minimize material usage, requiring efficient structural and chemical design. Designing multifunctional capsules with complex deformation should be possible even after minimizing the material usage through use of sparse fiber networks if the fibers are coated with responsive polymers.

Experiments: Here capsules are created with a shell made from a mesh of nanoscale bacterial cellulose fibers that provide mechanical strength at very low mass levels, while a coating of thermoresponsive Poly(*N*-isopropylacrylamide), PNIPAM, on the fibers provides control of permeability, elastic response, and temperature response. These properties are varied by grafting different amounts of polymer using particular reaction conditions.

Findings: The addition of PNIPAM to the cellulose mesh capsule enhances its mechanical properties, enabling it to undergo large deformations and recover once stress is removed. The increased elastic response of the capsule also provides reinforcement against drying-induced capillary stresses, limiting the degree of shrinkage during dehydration. Time-lapse microscopy demonstrates thermoreversible swelling of the capsules in response to temperature change. Cycles of swelling and shrinkage drive solvent convection to and from the capsule interior, allowing exchange of contents and mixing with the bulk fluid on a time scale of seconds. Because the cellulose capsules are produced via emulsion-templated fermentation, the polymer-modified biocapsule concept introduced here presents a pathway toward the sustainable and scalable manufacture of multifunctional responsive capsules.

* Corresponding author.
E-mail address: p.spicer@unsw.edu.au (P.T. Spicer).

https://doi.org/10.1016/j.jcis.2024.08.231
Received 26 May 2024; Received in revised form 6 August 2024; Accepted 27 August 2024
Available online 4 September 2024

Nomenclature

BIBB	α-bromoisobutyryl bromide	NA	Numerical aperture
CLSM	Confocal laser scanning microscopy	PNIPAM	Poly(*N*-isopropylacrylamide)
DMSO	Dimethyl sulphoxide	RhB	Rhodamine B isothiocyanate
FTIR	Fourier transform infrared	SEM	Scanning electron microscope
HMTETA	1,1,4,7,10,10-hexamethyltriethylenetetramine	TEA	Triethylamine

1. Introduction

The micro-encapsulation and subsequent release of active ingredients is central to the function of biological systems, such as the controlled release of DNA from pollen [1]. Similarly, synthetic systems are used to release active ingredients like therapeutics by osmotic or thermal triggers [2,3], though controlled release is an ongoing challenge [4]. Responsive microcapsules that have the capability to deliver their payloads on command have potential applications in pharmaceuticals [5], foods [6], and cosmetics [5], leading to significant research into new mechanisms of creating and triggering response [7–9].

A common response in capsules is rupture and release of contents triggered by osmotic pressure and this relies on the rigidity and low permeability of solid shells made of polymers [10,11], polymer blends [9], or metals [12]. One limitation of burst-release capsules is they are single-use and require diffusion of any released cargo through the surrounding liquid [7] at a rate dictated by solute size and fluid viscosity [6]. Accelerated dispersion of these payloads has been identified as an important component of microcapsule design [13,14] and a new development is microcapsules that can undergo repeated contraction and expansion in response to applied temperature, chemical, and magnetic fields [15–18]. All of these capsules, however, use solid shell structures that set an upper limit on their deformation and permeability.

We are interested in how a random fiber mesh can perform as a capsule shell, as it offers an efficient use of mass, provides ample surface area for reactive modification, and can undergo extreme deformation without mechanical failure. A new process enables production of such capsules by emulsifying a bacterial culture of *Acetobacter xylinum* in a gelled oil phase, a single-step and easily scaled biosynthesis [19] that templates a cellulose fiber mesh onto droplet interfaces [20]. Previous work converted the cellulose fiber shells into responsive chemically-fueled motor particles using a metal-oxide, MOF, coating to generate oxygen bubbles and propel the capsules through chemical fuel. The low density and high flexibility of the capsule shells allowed them to move through constrictions by deforming in ways not possible for solid particles or capsules [21].

Building on the easy synthesis and modification of such flexible capsule substrates, here we enhance the shell of cellulose microcapsules [19] via a grafting-from polymerisation of the thermoresponsive poly(*N*-isopropylacrylamide), PNIPAM. PNIPAM undergoes a swollen-to-collapsed transition in water as the temperature is increased above 32 °C [22,23]. The addition of PNIPAM adds unique responsiveness to the capsules, enabling swelling, permeability, and fluid pumping to be controlled by external stimuli, just as others have done with solid shells and hydrogel particles [15–17]. Here, however, the capsules are made of a thin shell of micron-length and nanometer-thick cellulose fibers in a mesh with a very low mass, ~100 ng, relative to conventional solid shells, making them highly responsive in shape and permeability.

Our approach enables tuning the thickness of the polymer film on the fibers and consequently the pore size of the hybrid capsule. Repeated cycling of temperature above and below the PNIPAM volume transition produces significant bulk flow into, out of, and around the capsules. The magnitude of response can be tuned by variation of the amount of grafted PNIPAM. The polymer coating on the cellulose fibers also improves their mechanical properties, as dried and flattened capsules can be rehydrated to completely recover from extreme deformation and revert to their original shape and size. This work demonstrates the viability of sparse fiber shells as mechanically stable capsules that can responsively contain, release, and mix their contents. The generality of the approach means the capsules could be used with other chemical surface coatings, expanding their applications.

2. Results and discussion

Bacterial cellulose microcapsules are synthesized by encapsulating drops of aqueous bacterial cellulose-producing culture in gelled oil [19]. The bacteria produce hollow, porous capsules from micron-scale cellulose fibers by templating onto the droplet interface, Fig. 1. The cellulose in the capsule shell is significantly entangled, as demonstrated by SEM and the long term stability of the capsules in sterile water. Adding PNIPAM to the surface of the capsule's cellulose fibers imparts a temperature-controlled change in the effective fiber size, Fig. 1 [22,23] that can be used to vary capsule permeability and shape but also drive secondary effects like fluid flow. The individual cellulose fibers in the mesh of the capsule shell were coated with PNIPAM using a two-step process: covalent attachment of polymerization initiator (BIBB) and then grafting of PNIPAM from the attached BIBB, Fig. 1. Further development of this platform would see the complexity of the polymer functionalization step reduced, likely via a grafting-to pathway.

2.1. Capsule characterization

We establish the presence of tethered PNIPAM layers through Fourier-transform infrared, FTIR, spectroscopy with results shown in Fig. 2. The peaks at 1450 cm^{-1}, 1525 cm^{-1} and 1650 cm^{-1}, which can be attributed to the stretching of the C-N, amide (II), and amide (I) bands, respectively, are characteristic absorption bands of PNIPAM. The peaks in the 2800–2980 cm^{-1} region correspond to the asymmetric and symmetric stretching of methylene (CH_2) groups in long alkyl chains. A sharper peak was observed at 1054 cm^{-1} that can be ascribed to the oxygen-containing groups of CO stretch. The absorption peak in the range of 1605–1657 cm^{-1} represents the CO stretch. The appearance of these characteristic peaks in the spectra of the modified cellulose microcapsules verifies successful grafting of PNIPAM [24].

Polymer thickness can be tuned by varying the reaction time and reaction rate. Scanning electron microscopy (SEM) was used to examine the change in fiber diameter upon grafting PNIPAM to the capsules, with representative images shown in Figs. 3 a-l. After polymerization, the average fiber diameter increased from 60 nm [19] to over 800 nm based on SEM data of freeze-dried samples, Table 1. At low polymer layer thicknesses, 'webbing' is observed at intersection points between the fibers and there appears to be a greater tendency for small fibers to stick together. As the polymer thickness increases further, individual fibers are no longer observed. A transition between coated fibers and regions of continuous polymer-fiber mats occurs between samples 2 and 4 for polymer thicknesses of 160–450 nm.

We note that it is difficult to calculate the precise amount of grafted PNIPAM in our system, as our chemistry does not allow for the polymer chains to be degrafted and measured, and thermal decomposition methods are not viable due to the organic nature of the cellulose substrate. As the bromination step was consistent across all capsules studied, we anticipate that the grafting density is relatively uniform across all samples and the differences in measured polymer thickness are proportional

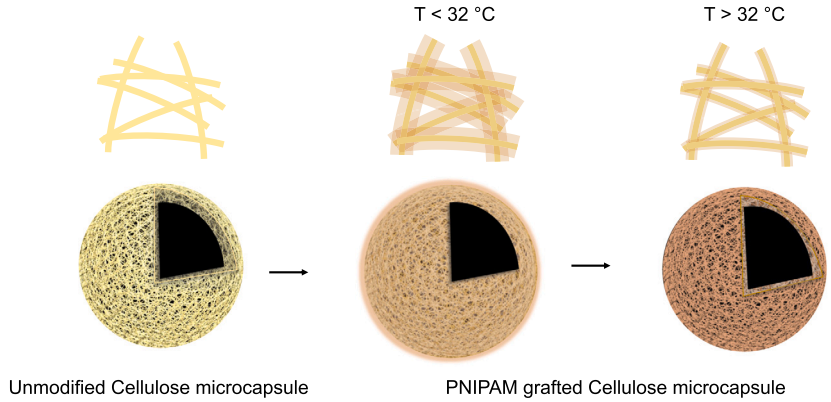

Fig. 1. Schematic of the functionalization of a cellulose microcapsule with surface-grafted PNIPAM. The fiber coatings can then be swelled and shrunk using changes in temperature to induce thermoreversible swelling of the PNIPAM.

Table 1
Polymerization conditions that produced the variety of functionalized microcapsules used in this work.

Reaction	A		B		
Sample number	1	2	3	4	5
Water/Methanol ratio	1:2	1:2	2:1	2:1	2:1
Reaction time (min)	15	30	15	30	75
Target thickness (nm)*	10	20	35	60	95
Fiber thickness (nm)†	140 ± 30	160 ± 30	300 ± 100	450 ± 150	850 ± 150
Shell thickness (μm)§	30	45 – 50	80	112	140

* Based on equivalent synthesis on planar silicon substrates via the method of Humphreys et al. [23].
† Fiber thickness from SEM images taken post polymerisation. Samples are freeze-dried before imaging to depict the porous structure of the capsules and the thickness of the cellulose fibers after coating with PNIPAM.

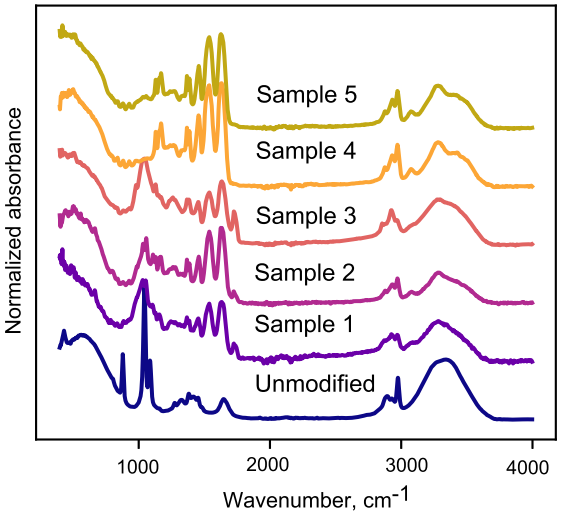

Fig. 2. FTIR spectra of cellulose microcapsules corresponding to the samples presented in Fig. 3. Absorbance peaks at 1450 cm^{-1}, 1525 cm^{-1} and 1650 cm^{-1} indicate the presence of PNIPAM and generally intensify with increasing sample number, agreeing with the trend presented in Table 1.

to differences in polymer molecular weight. However, as we cannot be certain of this, and are similarly uncertain regarding the polydispersity of the chains, we subsequently refer to the difference in PNIPAM coatings as a difference in polymer amount (mass per unit area). One factor that must be considered when calculating the amount of grafted polymer from the SEM images is the density of freeze-dried PNIPAM, which is unknown.

Variations in density are a likely cause of the significant, yet consistent, discrepancy between the target polymer thickness based on syntheses from silica wafers [23] and the thickness measured via SEM, Table 1. It is also possible that the polymerization process binds small cellulose fibers together, resulting in the larger fiber thicknesses observed in the polymerized samples, for example Fig. 3 b, c versus Fig. 3a. One additional factor to consider is the tendency for confined environments to accelerate ATRP [25]. The SEM images in Fig. 3 show that the amount of grafted PNIPAM consistently increases but cannot reveal the absolute amount of grafted PNIPAM. It is worth noting that the capsules are washed rigorously after functionalization, and stored in room-temperature water, in which free PNIPAM is readily soluble, for many days before the images in Fig. 3 were captured. The PNIPAM-fucntionalized cellulose surfaces observed by SEM are similar to those seen by Wu et al. [26], who grafted PNIPAM onto the larger fiber cellulose structure of filter paper, producing fiber surfaces covered with a layer of polymer. Wu et al. also found a smoother surface structure after increasing the percentage of polymer grafted, likely due to similar increases in connectivity of the PNIPAM regions as we see in Fig. 3 [26–28]. Taking the FTIR measurements together with SEM images and past observations, we are confident of successful covalent functionalization of the cellulose microcapsule substrate with PNIPAM.

Confocal laser scanning microscopy, CLSM, images demonstrate the effect of the polymer coating level on the thickness of the microcapsule shell in water, Figs. 3 m-r. In these measurements, a Rhodamine B stain, colored purple in the images, labels the fibers within the microcapsule. The confocal images are of a single plane in the middle of the capsule, indicating a hollow capsule with a wall thickness of 20–25 μm before polymerization, Fig. 3m, in agreement with [19]. The dark region inside the capsule wall in Figs. 3 m-r is a hollow core that could be used to carry a payload of particles or molecules, for example. The images in Figs. 3 m-r focus on the capsule shell and show the effect of polymerization time and reaction rate at this length scale of the capsules.

Increasing either reaction time or reaction rate increases the polymer coating thickness, in turn reducing the capsule pore size. Although

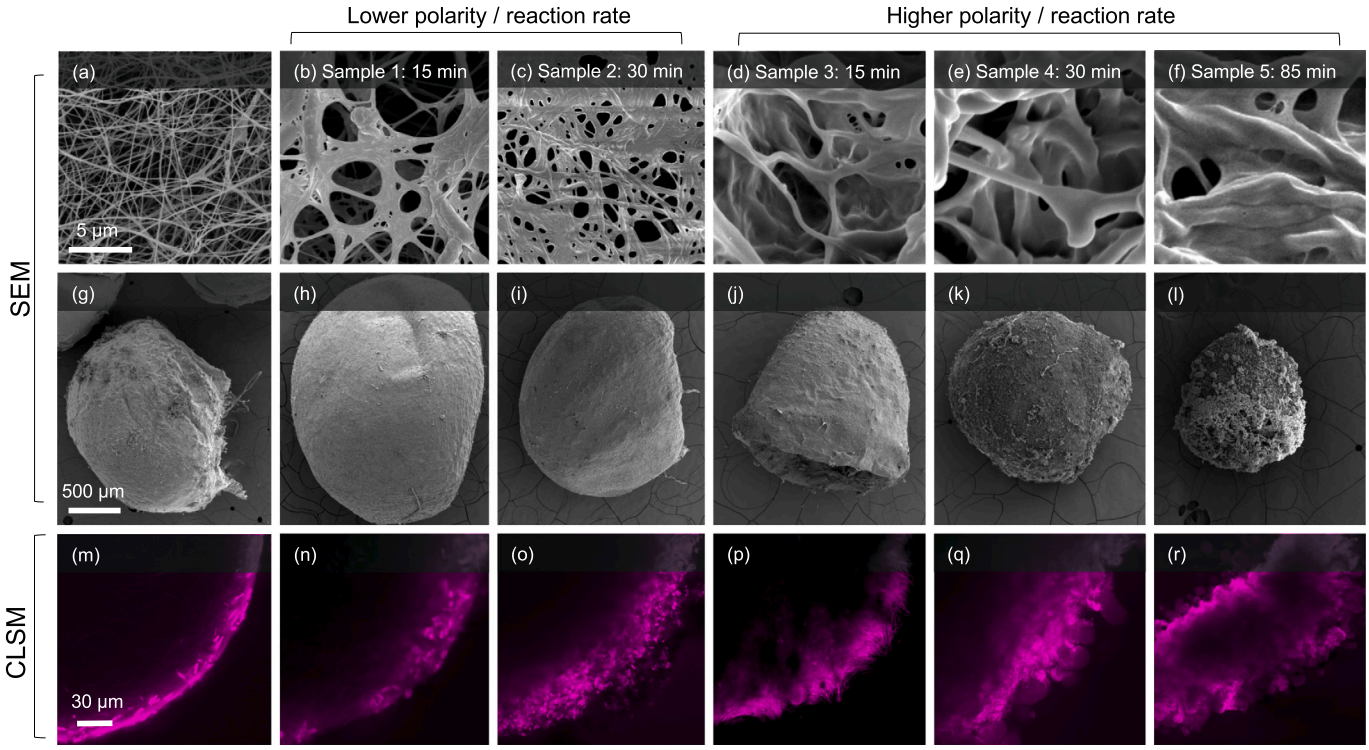

Fig. 3. SEM images of pristine and polymer-modified cellulose microcapsules. The target polymer thickness increases with increasing sample number; further details can be found in Table 1. (a-l) SEM images of freeze-dried microcapsules, illustrating that polymerization significantly increases the fiber thickness and modified the capsule nanostructure. (m-r) Confocal microscopy of cellulose microcapsules (m) stained with Congo red and (n-r) functionalized cellulose capsule, with PNIPAM stained with Rhodamine B. (For interpretation of the colors in the figure(s), the reader is referred to the web version of this article.)

Sample 1 and Sample 3 are produced using the same reaction time, the higher reaction rate of Sample 3 produces a larger PNIPAM coating, resulting in 2.1 times thicker fibers and 2.6 times thicker capsule walls along with smaller pore sizes, Fig. 3. As the polymerization time increases for both high and low polymerization rates, we observe that the thickness of the fibers, Figs. 3 a-f, and the wall of the microcapsule increase, Figs. 3 m-r, by a factor of 10 for the maximum reaction time and the polymerization rate for Sample 5 (Table 1). The range of PNIPAM amounts deposited on microcapsules in this study spans a range allowing control of capsule dimensions but also other properties like the amount of water absorbed and released during temperature cycles. As a result, the capsules can be designed to exhibit changes at both bulk and micron length scales.

2.2. Permeability

The permeability of PNIPAM-functionalized microcapsules in water at 25 °C and 45 °C was examined by soaking a microcapsule in aqueous solutions of FITC-labeled dextran with specific hydrodynamic radii. The permeability of dextran into, or exclusion from, the capsules reflects a molecular size cutoff due to the relative pore size versus the hydrodynamic radius of the dextran tracer. To capture and quantify FITC-dextran transport, confocal or fluorescent microscopy can be used to measure the fluorescence intensity of FITC-dextran inside and outside of the capsule. Here, the molecular size exclusion of the PNIPAM-functionalized microcapsules was studied. PNIPAM-functionalized microcapsules were equilibrated for 12 h in 4 kDa FITC-labeled dextran with a hydrodynamic radius of approximately 1.8 nm in water (Fig. 4) [9,29,30].

Figs. 4 (a-d) show mid-plane images of FITC-labeled dextran fluorescing in green, with high-intensity pixels corresponding to a higher concentration and black regions indicating the absence of the tracer molecule during observation. The increase in the thickness of the PNIPAM coating results in a decrease in the internal intensity of FITC-dextran, signifying a reduction in capsule pore size due to the added PNIPAM. The capsule made by the Sample 2 method shows some transport of FITC-dextran into its core, with some increased concentration as the capsule is heated, Figs. 4 a and c. For the Sample 4 capsules, however, no FITC-dextran can be detected inside the capsule, Fig. 4b. Compared with the pristine cellulose microcapsule, the pore size has significantly reduced from the 500 nm reported by Song et al. [19] to less than approximately 1.8 nm at room temperature. Since PNIPAM is thermally responsive, an increase in temperature above 31 °C causes the thickness of the PNIPAM coating to shrink, increasing the capsule pore size, which allows penetration of 4 kDa FITC-dextran. Fig. 4 c demonstrates that the internal intensity of Sample 2 increased at 45 °C, while Sample 4 remained unchanged; in both cases, the same capsule was studied after elevating the temperature, but some movement may have occurred.

The normalized intensity of all five samples is plotted at both 25 °C and 45 °C, Fig. 4 e. The trend of increasing the capsule's internal intensity with temperature was observed consistently as it will always increase the pore size and permeability of a given capsule. However, increasing the PNIPAM coating by different reaction conditions in Sample 4, Figs. 4 b and d, changes the size cutoff, making the synthesized capsule impermeable to 4 kDa dextran, even after raising the temperature to 45 °C. Clearly the larger PNIPAM coating is sufficient to block passage of the 1.8 nm FITC-dextran even after temperature-induced shrinkage. The temperature response of the capsule coatings can be tuned depending on the transport properties desired for a given application. One could also imagine using the polymer grafting reaction as a way of sealing the contents of the capsule to prevent release. Release could then be triggered by heating.

2.3. Deformation and shape memory

Due to the low solid density and small characteristic length scales of the cellulose microcapsules, drying the capsules causes significant changes in their size and shape due to strong capillary forces [19]. Here

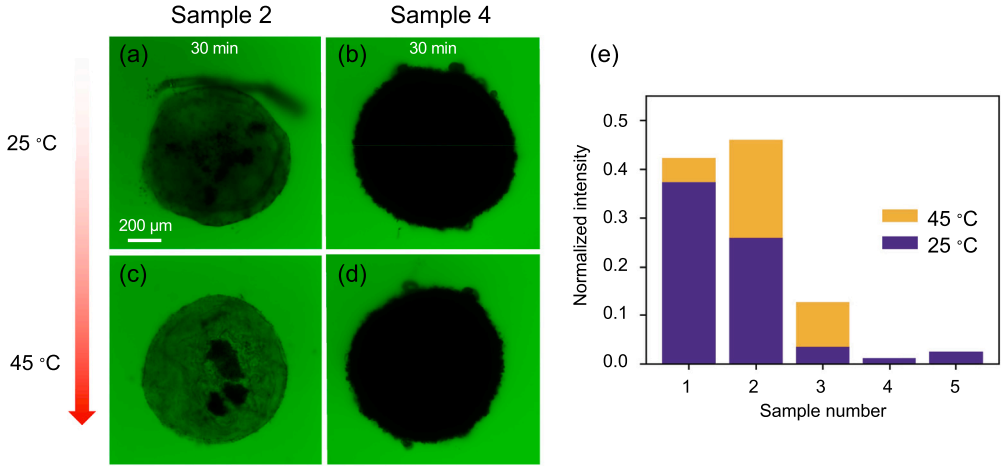

Fig. 4. Effect of PNIPAM functionalization on cellulose capsule permeability at 25 and 45 °C. (a-d) CLSM images of the middle plane through the polymer-modified cellulose microcapsules incubated in 4 kDa FITC-labeled dextran at 25 °C (a and b) show that increasing polymer thickness decreases capsule permeability. Also, increasing the temperature from 25 °C to 45 °C enhances the capsule permeability at low polymer thickness only (c). The capsule with thicker PNIPAM coating remains impermeable to 4 kDa FITC-labeled dextran even after increasing the temperature. (e) Fluorescence intensity is normalized by dividing the average intensity inside the capsule by the average background intensity of the external fluid, quantifying the variations observed in a-d as well as other samples.

we investigate the deformation and recovery of PNIPAM-functionalized microcapsules during drying and rehydration to understand any enhancements in the hybrid capsule response.

During drying, the pristine cellulose capsules collapsed completely into a flat disk ~100 nm thick, Fig. 5. The dried thickness is less than 1% of the initial hydrated capsule radius Fig. 5a, consistent with past work [19,21,31]. Similar behavior was observed for Samples 1 and 2, which had smaller amounts of PNIPAM attached, with the capsules collapsing to a thin disk upon drying, Fig. 5a. For the thicker PNIPAM coatings on Samples 3-5, a remarkable difference is evident in the capsule drying behavior. The increased PNIPAM coating allows the capsules to maintain most of their volume upon complete dehydration, presumably due to a significant increase in elastic modulus that can offset the capillary stresses during drying.

Capillary force dominates the observed compression of the cellulose capsule structure during drying [19,32]. This force induces crumpling as the cellulose fibers dynamically reconfigure to minimize the area of the energetically unfavorable solid/air interface. As liquid continues to evaporate, the capsule undergoes further deformation, with maximum capillary tension occurring when the meniscus radius is small enough to just fill the pores between fibers [33]. Throughout the drying process, capillary forces draw the fibers into physical contact [34], where strong hydrogen bonds and van der Waals interactions can cause the fibers, if not coated, to irreversibly bind [35,19].

Coating cellulose fibers, even at low PNIPAM levels, interrupts the typically irreversible attachment of the cellulose fibrils to one another during drying, akin to the protection afforded by the adsorption of carboxymethyl cellulose polymer [35], although the latter effect is lost by polymer dissolution upon rehydration. Due to the polymer's strongly-bound protection of fiber surfaces, drying of PNIPAM-cellulose microcapsules is an easily reversible process, allowing them to reswell upon rehydration. Previous work by Song et al. [19] demonstrated that pristine cellulose microcapsules cannot reswell upon rehydration, instead remaining as a thin collapsed disk. In contrast, all dehydrated PNIPAM-functionalized capsules studied here reswelled to their initial shape and size upon water immersion, even after an enormous compression during drying. We observed that this collapse/reswelling behavior remained consistent across at least five drying/rehydration cycles, indicating that reuse is an additional benefit of the robust PNIPAM coating. It also implies that these capsules have the potential to reversibly transition over several orders of magnitude in size, between millimeter and micron length scales, due to their low-density shell structures.

An additional demonstration of the flexibility of the PNIPAM cellulose capsules under stress is shown by their shape recovery after compressive deformation by a blunt capillary. Song et al. [19] found that pristine cellulose capsules could only recover from less than 20% strain, with greater deformation permanently altering the shape of the capsule. Building on this, Hosseini et al. [21] showed that coating the capsules with MOFs allowed them to propel themselves through chemical fuel solutions, while their deformability allowed them to squeeze through constrictions that would impede solid particles. The addition of the crystalline MOFs increased the maximum strain the capsules could experience, easily compressing by 35% in tight channels [21].

Here attachment of PNIPAM to the cellulose network greatly improved the post-deformation shape-recovery of the capsules. In Fig. 5, the PNIPAM-functionalized microcapsule from the Sample 2 batch recovers to 88% of its initial shape after even 100% deformation. This recovery occurred quickly, generally within five seconds after removal of the applied stress, and was independent of the initial deformation rate and reproducible over at least five cycles of deformation. The PNIPAM clearly alters the elastic response of the capsule through mechanical reinforcement of the cellulose fibers, as PNIPAM hydrogels have a high elastic modulus of 45 kPa before the phase transition [36]. The cellulose microcapsules have an elastic modulus of only 100 Pa [19]. It is worth noting that the improved elastic recovery from deformation imparted by the grafted polymer is likely not specific to PNIPAM and could be realized by grafting other polymers to the cellulose structure. This generalized hybridization approach could be used to yield more complex functions by adding pH-responsive polymers [37,38] or PEG groups that also add protection from biological targeting of the capsules [39], for example.

2.4. *Changes in capsule volume with temperature*

Capsules undergoing reversible volume transitions can perform payload delivery and even 'swim' via jellyfish-like contractions [40]. We are interested in the performance of our sparsely structured capsules as they undergo the same sort of volume transition in the thin NIPAM surface coating on the underlying cellulose nanofiber scaffold structures. Here we imaged capsules undergoing temperature cycling between 23 °C and 40 °C at a constant rate of 20 °C min^{-1} to quantify the dynamics of microcapsule response. Figs. 6a-c show composite bright-field microscopy images [14] that highlight in orange the areas where the PNIPAM-functionalized capsule boundary moves during contraction in a 30 s temperature cycle, Figs. 6a-c. While the images are obtained in

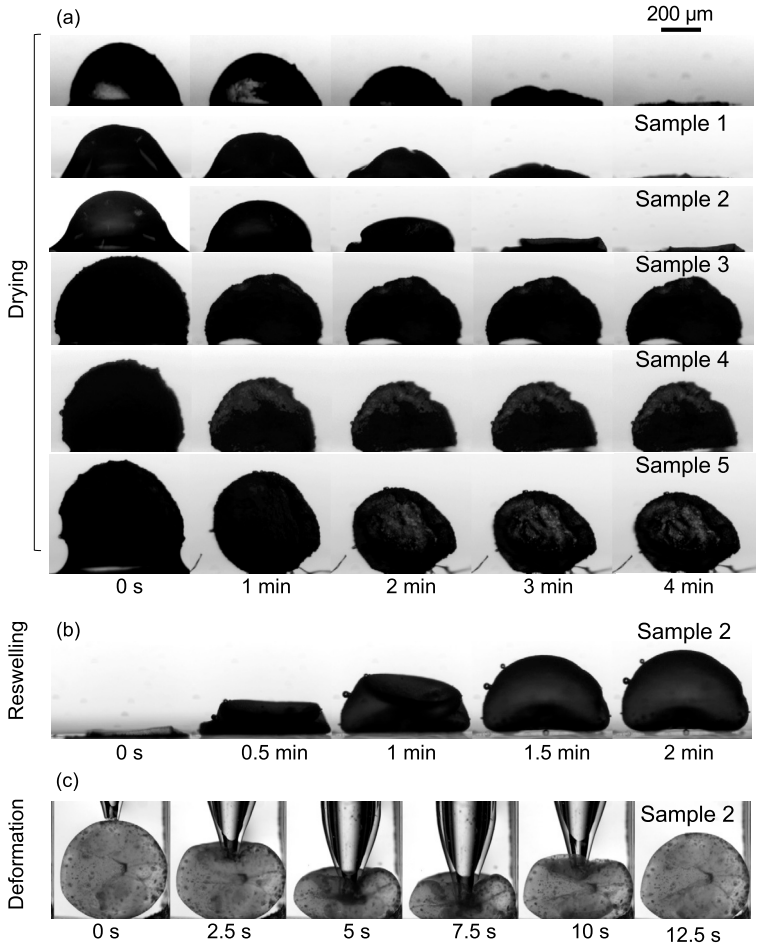

Fig. 5. (a) Air drying of cellulose microcapsules before and after coating with PNIPAM. Cellulose capsules can collapse to a flat sheet during drying; however, the thickness of the final air-dried sheet increased with additional attached PNIPAM amounts. Samples 3-5 do not fully compress upon drying as their PNIPAM coating reinforces them to a greater extent. (b) All PNIPAM-cellulose capsules reswell after immersion in water, but the pristine cellulose capsule does not. (c) Functionalized capsule (Sample 2) recovery after compressive deformation with a blunt-end glass microcapillary.

grayscale, false coloring is used to highlight only areas where the image changes, allowing us to quantify the distance moved in a known time and, thus, the velocity.

Measurement of the area of the polymerized capsule with image analysis quantifies the degree of change for each capsule type, Figs. 6d-e. The change in the area of capsule with the thinnest PNIPAM coating, Sample 1, is ~4%, while Sample 4 changes by ~13%, Fig. 6e, corresponding to volume changes of ~6 and ~19%, respectively. All PNIPAM-coated capsules were thermoresponsive, with the magnitude of the area change varying with the amount of grafted PNIPAM, as can be seen from Fig. 6e. Sample 5, which has the highest amount of PNIPAM coating, shows a greater change in area during temperature cycling compared to Sample 1, which has the smallest amount of PNIPAM.

The amount of movement is small relative to the overall dimensions of the capsule, but this makes sense as the amount of solid mass present is quite low and mostly in the shell of the capsule. So if we consider the motion relative to the shell thickness, we see how this dimension dominates the motion. Sample 1, for example, has a shell thickness of 30 µm and the range of motion exhibited in Fig. 6a is 18 µm - 40 µm. On a shell thickness basis the motion is significant and consistent with fully solid PNIPAM particles similar in size to the capsule wall thicknesses here [41,42]. Similarly, for Sample 2 we have a shell thickness of 50 µm and a motion of 15 µm - 50 µm. For Sample 5 the thickness is 140 µm and the motion is 30 µm - 60 µm. The fact that the Sample 5 capsule with a higher coating of PNIPAM moves less indicates the motion is partially constrained by the elasticity of the underlying cellulose fiber structure. The volume transition is reversible over four hot-cold cycles with and may have some hysteresis, Fig. 6d, as the minimum and maximum area systematically increase over time. Such gradual change may be due to some structural rearrangement or compliance.

As the PNIPAM coating level increases from Fig. 6a-c, the perimeter of the capsule becomes increasingly irregular in appearance. As these images highlight changes in volume of the capsule, the irregularity might be perceived as wrinkling or buckling but is actually a result of excess PNIPAM spheres on the capsule surface, as we confirm by SEM imaging, visible in Fig. 3l and Fig. S4. These spheres provide a nice independent check of the volume change of the PNIPAM without cellulose present as they shrink by 40% in diameter, consistent with earlier work on solid PNIPAM hydrogels [41,42].

Despite the relatively small change in volume during the above temperature-induced transitions, repeated cycling of the microcapsules can cause significant fluid flow in the immediate environment. The flow is influenced by three factors during temperature cycling: the radial displacement of the microcapsule, the adsorption and expulsion of water by the PNIPAM, and changes in the PNIPAM-cellulose microcapsule pore size. The three effects cause a net flow towards the capsule when swelling occurs and away from the capsule when shrinkage occurs. This is initially counter-intuitive because the net motion of the fluid is in the opposite direction to the motion of the capsule wall. But, as Fig. 6f shows, the motion of the wall is relatively small but displaces significant volume of fluid in the opposite direction, driving the net flow observed. This makes sense since the small linear motion translates into a rela-

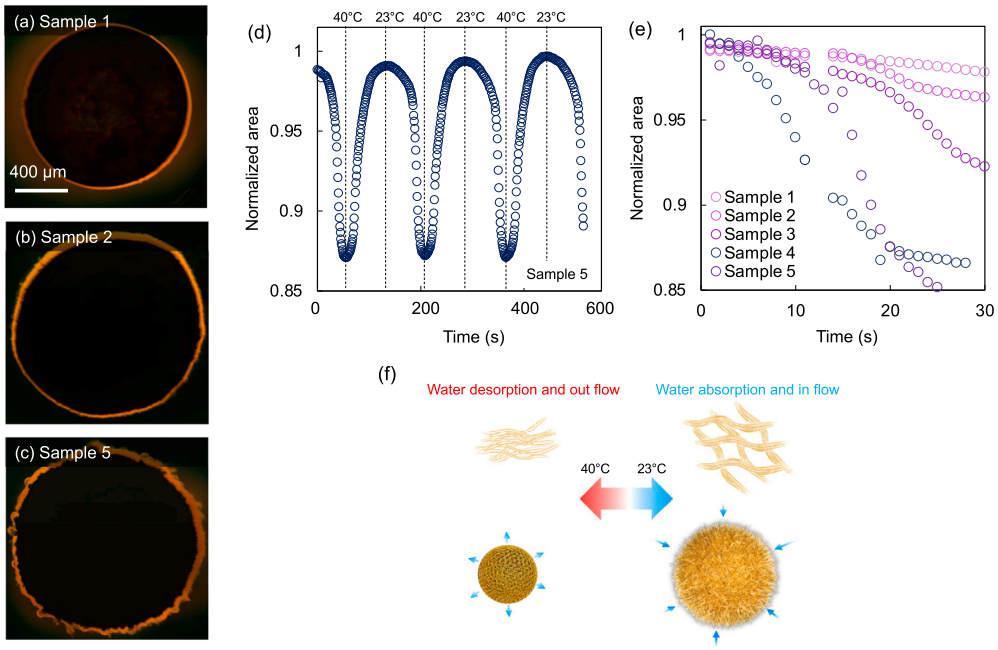

Fig. 6. (a-c) Composite images of PNIPAM-cellulose microcapsules undergoing thermoreversible swelling. The orange regions highlight the areas of greatest deviation of position between the initial image at 23 °C and a final capsule image at 40 °C over 30 s. (d) Multiple cycles of temperature-induced area change 23 and 40 °C, PNIPAM modified capsule shows the same rate for each polymerization time in each cycle. (e) Increasing the amount of PNIPAM increases the volume transition magnitude and rate. (f) Schematic of the PNIPAM polymerized capsule volume transition releasing and absorbing water.

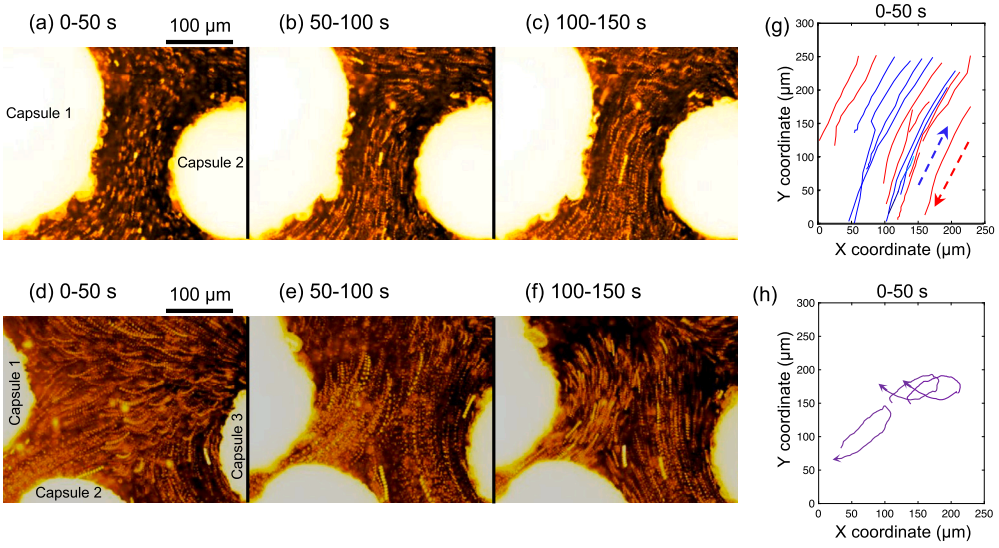

Fig. 7. Fluid mixing using PNIPAM-cellulose microcapsules during contraction and relaxation: Time-lapse of streamlines around two (a-c) and three (d-f) PNIPAM-cellulose microcapsules (sample 5) during contraction and swelling in response to temperature cycling from 25 to 40 °C. Representative trajectories (g and h) of the 3 μm tracer in the bulk fluid around (g) two and (h) three capsules made via Sample 5 methods. Blue and red arrows indicate cooling and heating cycles, respectively.

tively large volumetric movement, where a movement of the wall of a 1 mm diameter capsule over 30 μm, for example, displaces about 15% of the fluid volume in the capsule. We are also interested in the collective influence of these capsules on bulk flow.

2.5. Particle tracking during multiple cycles of temperature change

Fig. 7a-c illustrates in- and out-flow of the bulk fluid caused by temperature-induced expansion and shrinkage of the PNIPAM-cellulose capsules. Here 3 μm tracer particles were employed to highlight bulk fluid movement flow around the capsules during temperature cycling. Light microscopy was utilized to capture the tracer motion and the images in Fig. 7 were created from combined multiple frames for each temperature cycle. For each temperature cycle, Figs. 7a-c and Figs. 7d-f, the system is taken from 25 °C to 40 °C at a rate of 20 °C/min to capture the effects of capsule shrinkage on local flow. Figs. 7a-c each display 50 sec blocks of time for two capsules made using the Sample 5 method. The results reveal that the motion of tracers is influenced by the motion of both capsules, resulting in linear forward and backward motion of the tracers. Fig. 7g shows individual tracer particle trajectories to highlight the alignment of the flow and the direction followed between the capsules. When three microcapsules were used, Fig. 7d-f, tracers exhibited rotational motion, providing the chaotic flow required for fluid mixing

[43]. Several trajectories are plotted in Fig. 7h to highlight the length scale of fluid recirculation achieved.

Tracking individual tracers and measuring their average velocity showed an average velocity of 42 μm/sec when three capsules were used, while the lowest velocities were observed for a single microcapsule (4 μm/sec). These velocities are faster than the speed of the capsule wall motion measured in Fig. 6e. We can use a similar approach to characterize the enhancement of flow by the porous structure of the capsules. A capsule wall velocity of 3.4 $\mu m\, s^{-1}$, for example, produces a local radial tracer velocity outside the capsule of 4 $\mu m\, s^{-1}$. The acceleration results from the porosity of the capsule, as there is more capsule surface area moving during shrinkage than the area of pores available for fluid flow. The coupling between the thermally triggered release of capsule contents and the convective mixing of the material with the external fluid is an interesting aspect of the capsules' potential applications. Mixing of capsule contents with the fluid environment, for example, could lead to improved and controllable transport rates over much larger dimensions than diffusion would enable.

3. Conclusions

In this study, multifunctional microcapsules were developed by coating the fibrous structure of bacterial cellulose microcapsules by attaching an initiator and grafting a thermal-responsive polymer to the fibers. The resulting PNIPAM-modified capsules exhibited a porous and flexible structure, providing unique functionality beyond existing encapsulation systems. The thickness of the PNIPAM coating influences capsule permeability and volume transitions and was controlled by adjusting reaction rates and times during polymerization. The synthesized capsules demonstrated mechanical robustness and the ability to recover their initial shape after dehydration and deformation despite a very low solid density. The large size of the capsules enables the containment of a significant volume of fluid, and their tunable permeability allows for the temperature-triggered release and mixing of a payload during temperature changes.

The flow around the PNIPAM-modified capsules was visualized by tracking tracer particles, highlighting their potential for enhanced release and mixing of the capsule contents or adjacent fluid. Despite their low mass, the capsules possess sufficient strength to perform multiple functions by utilizing temperature variations as a trigger. These capabilities make them promising for applications such as micromixing and controlled uptake and release. The synthesis method is general enough to be used for other polymer coatings to provide broader responses as well as other functions like chemically-driven propulsion [21].

4. Materials and methods

4.1. PNIPAM-cellulose capsule synthesis

4.1.1. Cellulose microcapsule preparation

Cellulose microcapsules with diameters in the range of 50–1000 μm were synthesized by a previously developed bio-interfacial process [19]. In brief, bacterial cellulose microcapsules were grown using a monodisperse emulsion of bacterial culture droplets as templates. The bacterial culture contains purified *Acetobacter xylinum* that was purified and concentrated from Kombucha culture (Nourishme Organics, Australia) by gradient centrifugation. Coconut water (Cocoa, Indonesia), and 10% w/v table sugar were added as nutrients to create water-in-oil emulsion drops. After 10 days of incubation, the encapsulated bacteria convert the glucose molecules into cellulose nanofibers with a diameter of 60–70 nm, that then entangled around the droplet to form an interconnected fiber mesh with a total thickness of 20–50 μm, a pore size of 0.5 μm, and bulk density of 0.01 $g\, cm^{-3}$ [19,21]. Bacterial cellulose microcapsules are harvested by heating the emulsion to 90 °C for 2 hours to remove the oil yield stress, followed by separating the oil and water phases, during which the cellulose microcapsules settle into the bottom water phase. At this stage, most of the bacteria are dead. The bacterial cellulose microcapsules are then soaked in 2% w/v NaOH (Chem-Supply Pty Ltd, Australia) overnight and washed with deionized water at least three times to remove any dead bacteria and other impurities [19].

4.1.2. Dehydration of cellulose microcapsules

The washed cellulose microcapsules were placed into a 15 mL Falcon centrifuge tube and allowed to settle before the supernatant was drawn off with a syringe, leaving ~0.5 mL remaining. The Falcon tube was then filled with THF (Tetrahydrofuran, ≥99%, Sigma Aldrich) and gently mixed. After the microcapsules settled, the supernatant fluid was drawn off and more THF added. The solution was exchanged in this manner five times; leaving $\sim 1.23 \times 10^{-4}$ vol% water remaining in the solution. After this, the microcapsules were transferred to a 5 mL glass vial which was filled with anhydrous THF (dried over 4 Å molecular sieves) and the top stoppered with cotton wool. The stoppered 5 mL vial was then placed into a 50 mL vial containing 4 Å molecular sieves that was then filled with more anhydrous THF. The 50 mL vial was stoppered with a suba-seal and left overnight, allowing residual water from the solution to be adsorbed by the molecular sieves.

4.1.3. Attachment of polymerization initiator

The microcapsules were transferred to a 5 mL vial that had been dried at 50 °C, which was subsequently filled with 3 mL of anhydrous THF and sealed with a suba-seal. Then 0.5 mL of TEA (triethylamine, ≥99%, Sigma Aldrich) was added to the vial, followed by 0.4 mL of BIBB (α-bromoisobutyryl bromide, ≥98%, Sigma Aldrich). Upon addition of the BIBB, a white precipitate formed and remained for the entire reaction time. The reaction was allowed to proceed for one hour, during which the BIBB reacted with the hydroxyl groups on the cellulose fibers, leaving them decorated with organobromine ATRP initiators. The reaction was halted by pouring the solution into a 50 mL vial containing 30 mL of ethanol, then microcapsules remaining in the 5 mL vial were removed by rinsing the vial with ethanol. The white precipitate dissolved in the ethanol solution, and the microcapsules were allowed to settle. The solution was then exchanged to methanol via the same method used for water-THF solution exchange in the previous step.

4.1.4. Polymerization

In this work the activators regenerated by electron transfer atom transfer radical polymerization (ARGET ATRP) method was used to graft PNIPAM from the cellulose framework of the microcapsules; our method is based off that of Humphreys et al. [23], which is reported to produce brushes with a grafting density of approximately 0.1 nm^{-2} [44]. The molecular weight of the grafted polymers is a function of both the polymerization time and the polymerization rate (K_{ATRP}); K_{ATRP} is accelerated as the solvent polarity is increased [45], which is dictated in our system by the ratio of water to methanol in the solvent. In this work we used two solvent compositions (water/methanol of 1:2 and 2:1, reactions A and B, respectively) and a number of reaction times to prepare polymer coatings with a range of polymer thickness. The polymerization solution was prepared such that there was 0.05 $mg\, mL^{-1}$ of PNIPAM in solution, and the molar ratio of PNIPAM to HMTETA (1,1,4,7,10,10-hexamethyltriethylenetetramine, ≥97%, Sigma Aldrich) to $CuBr_2$ (copper (II) bromide, ≥99%, Sigma Aldrich) to ascorbic acid (≥99%, Sigma Aldrich) was 900:10:1:6.6.

Before the polymerization the brominated cellulose microcapsules were placed in a methanol solution. These microcapsules were then placed into a 5 mL vial with a measured amount of methanol (here we assume that the microcapsule weight is negligible). The methanol solution was deoxygenated by purging with nitrogen for at least 15 minutes. Concurrently, a polymerization solution was prepared by dissolving PNIPAM in MilliQ water in a round-bottomed flask. To this solution, HMTETA and $CuBr_2$ were added according to the above molar ratios. A stirrer bar was then added and the flask sealed with a suba-seal.

The polymerization solution was deoxygenated by purging with nitrogen for 15 min, after which ascorbic acid was added to the solution, causing the color of the solution to change from pale blue to colorless. After a further fifteen minutes of deoxygenation, a calculated amount of the polymerization solution was syringed from the round-bottomed flask into the 5 mL vial containing the microcapsules in methanol. Water, methanol, and polymerization solution quantities were calculated such that this final solution possessed the solvent ratio, PNIPAM concentration, and reagent ratios outlined in the above paragraph. Functionalized microcapsules can be prepared in many vials simultaneously using this method, allowing the polymerization time to be varied for study of PNIPAM molecular weight effects.

After the allotted polymerization time, the microcapsules were transferred from the 5 mL vial to a 50 mL Falcon tube containing 30 mL of ethanol. The reduction of solvent polarity, exposure to oxygen, and rapid dilution effectively halted the polymerization. The capsules were allowed to settle before the supernatant liquid was removed. The capsules were washed in this manner twice more in ethanol before being transferred to MilliQ water via the solvent exchange method used above. The polymerization conditions corresponding to the microcapsules discussed in this work are summarized in Table 1.

4.2. Optical microscopy

Confocal light-sheet microscopy (CLSM) was used to image fiber networks and conduct flurescence measurements. A Zeiss LSM 880 microscope with Airyscan module was used for all CLSM measurements. A 63× oil immersion objective (numerical aperture of 1.4) was used for confocal imaging of polymerized fiber at room temperature and a 20× dry objective (numerical aperture of 0.16) was used for FITC-dextran permeability experiment. Rhodamine B (RhB, Sigma Aldrich) staining was used to visualize the tethered PNIPAM, and was carried out using the following established labeling protocol of Silverberg et al. [46]. First 2 mg of Rhodamine B (RhB) were dissolved in 2.5 mL of sodium carbonate-bicarbonate buffer (0.5 M, pH 9.5). Then, the RhB solution was added into 1 mL solution (water) containing the PNIPAM functionalized capsules (~85 capsules). The mixture was agitated overnight at room temperature in darkness. The capsule was rinsed with Milli-Q-water several times to remove any unattached dye.

Fluorescein isothiocyanate-dextran (FITC-dextran, Sigma Aldrich), with molar mass of 4 kDa, with respective hydrodynamic diameter of approximately 1.8 nm, was used as a fluorescent probe to quantify capsule permeability [47,3]. Polymerized capsules were immersed in a 2 mL solution of FITC-dextran with a concentration of 1 $mg\,mL^{-1}$. They were incubated at 25 °C for 24 h prior to imaging. Confocal fluorescence microscopy was then used to capture images of these microcapsules at room temperature. The fluorescence intensity was quantified using ImageJ [48] to determine the extent of permeation of the capsules by the dextran tracer molecule. Optical microscopy was used to observe the microcapsule response to temperature and mechanical deformation. Images were acquired using a stereoscope (WILD M3C, Leica, Germany) with a 6.4× objective, and an inverted optical microscope with a 10 and 40× objective along with a digital camera (Moticam 10 MP, Taiwan). The inverted optical microscope was equipped with a temperature-controlled stage (T96-P, Linkam) with a maximum heating and cooling rate of 20 °C min^{-1}.

4.3. Particle tracking

Polybead carboxylate green-dyed microspheres (Polyscience, Inc., Warrington, PA) with a diameter of 3 μm were employed to track and map the flow around functionalized capsules during their volume transition. The capsules were immersed in a water dispersion containing the tracer particles for a duration of 1 hour. The mixture of the tracer particles and polymerized capsules (sample 5) was introduced into a square capillary with a closed end (VitroCom) measuring 1 mm in side length. Particle displacement was tracked over time using image analysis techniques at room temperature and during temperature cycling between 23 and 40 °C. The velocity of the tracer particles was measured at an acquisition rate of 2 frames per second. Particle tracking was performed using the ImageJ software, and the TrackPy module [49] at 23 and 40 °C [50].

4.4. Fourier-transform infrared spectroscopy

FTIR absorption spectra were collected using a Bruker IFS66/S High-End FT-NIR/IR Spectrometer, which covered a wavenumber range from 400 cm^{-1} to 4000 cm^{-1}. The measurements were performed on air-dried microcapsules, which were placed onto the crystal surface with caution and secured using the pressure arm to ensure optimal contact. Prior to usage, the crystal was cleaned by thoroughly washing it with isopropyl alcohol to eliminate any potential contaminants or residues.

4.5. Scanning electron microscopy

Scanning electron microscopy (SEM) was utilized to verify the grafting of the polymer onto the microcapsules and examine the resulting nanostructures. SEM imaging was conducted using a FEI Nova Nano SEM 450 FE-SEM with an accelerating voltage of 5.0 kV. Before SEM imaging, the samples were rapidly frozen in liquid nitrogen, followed by overnight dehydration in a freeze drier. To enhance the sample's conductivity and improve imaging quality, a 30 nm thick platinum layer was deposited on the samples using a Leica ACE600 sputter coater.

CRediT authorship contribution statement

Maryam Hosseini: Writing – original draft, Visualization, Validation, Methodology, Investigation, Formal analysis, Data curation, Conceptualization. **Isaac J. Gresham:** Writing – original draft, Visualization, Validation, Investigation. **Stuart W. Prescott:** Writing – review & editing, Supervision, Conceptualization. **Patrick T. Spicer:** Writing – review & editing, Writing – original draft, Validation, Supervision, Resources, Project administration, Investigation, Funding acquisition, Conceptualization.

Declaration of competing interest

The authors declare the following financial interests/personal relationships which may be considered as potential competing interests: Patrick Spicer reports financial support was provided by Australian Research Council via DP190102614 and LE200100221. Isaac Gresham reports support was provided by AINSE Ltd. If there are other authors, they declare that they have no known competing financial interests or personal relationships that could have appeared to influence the work reported in this paper.

Data availability

Data will be made available on request.

Acknowledgements

MH acknowledges support from a UNSW Scientia PhD fellowship. IJG thanks the Australian Government and AINSE Ltd. for providing financial assistance for the period when this work was completed (Research Training Program Scholarship and PGRA Award, respectively). The authors also acknowledge partial support from the Australian Government through the Australian Research Council's Discovery Projects funding scheme, Project DP190102614, and the Australian Research Council's Linkage Infrastructure, Equipment and Facilities (LIEF) funding scheme, Project LE200100221.

Appendix A. Supplementary material

Supplementary material related to this article can be found online at https://doi.org/10.1016/j.jcis.2024.08.231.

References

[1] S. Werchner, E. Gute, C. Hoose, C. Kottmeier, A. Pauling, H. Vogel, B. Vogel, When do subpollen particles become relevant for ice nucleation processes in clouds? J. Geophys. Res., Atmos. (2022) e2021JD036340.

[2] S.-H. Kim, J.-G. Park, T.M. Choi, V.N. Manoharan, D.A. Weitz, Osmotic-pressure-controlled concentration of colloidal particles in thin-shelled capsules, Nat. Commun. 5 (1) (2014) 1–8.

[3] B. Kim, T.Y. Jeon, Y.-K. Oh, S.-H. Kim, Microfluidic production of semipermeable microcapsules by polymerization-induced phase separation, Langmuir 31 (22) (2015) 6027–6034.

[4] B.J. Boyd, D.V. Whittaker, S.-M. Khoo, G. Davey, Lyotropic liquid crystalline phases formed from glycerate surfactants as sustained release drug delivery systems, Int. J. Pharm. 309 (1–2) (2006) 218–226.

[5] S. Roberts, V. Miao, S. Costa, J. Simon, G. Kelly, T. Shah, S. Zauscher, A. Chilkoti, Complex microparticle architectures from stimuli-responsive intrinsically disordered proteins, Nat. Commun. 11 (1) (2020) 1–10.

[6] S. Boostani, S.M. Jafari, A comprehensive review on the controlled release of encapsulated food ingredients; fundamental concepts to design and applications, Trends Food Sci. Technol. 109 (2021) 303–321.

[7] J.M. Unagolla, A.C. Jayasuriya, Drug transport mechanisms and in vitro release kinetics of vancomycin encapsulated chitosan-alginate polyelectrolyte microparticles as a controlled drug delivery system, Eur. J. Pharm. Sci. 114 (2018) 199–209.

[8] J.G. Werner, B.T. Deveney, S. Nawar, D.A. Weitz, Dynamic microcapsules with rapid and reversible permeability switching, Adv. Funct. Mater. 28 (39) (2018) 1803385.

[9] T. Paulraj, A.V. Riazanova, K. Yao, R.L. Andersson, A. Müllertz, A.J. Svagan, Bioinspired layer-by-layer microcapsules based on cellulose nanofibers with switchable permeability, Biomacromolecules 18 (4) (2017) 1401–1410.

[10] Q. Meng, S. Zhong, Y. Gao, X. Cui, Advances in polysaccharide-based nano/microcapsules for biomedical applications: a review, Int. J. Biol. Macromol. (2022).

[11] K. Kempe, K.F. Noi, S.L. Ng, M. Müllner, F. Caruso, Multilayered polymer capsules with switchable permeability, Polymer 55 (25) (2014) 6451–6459.

[12] Y. Ping, J. Guo, H. Ejima, X. Chen, J.J. Richardson, H. Sun, F. Caruso, pH-responsive capsules engineered from metal–phenolic networks for anticancer drug delivery, Small 11 (17) (2015) 2032–2036.

[13] H. Tan, A. Banerjee, N. Shi, X. Tang, A. Abdel-Fattah, T.M. Squires, A two-step strategy for delivering particles to targets hidden within microfabricated porous media, Sci. Adv. 7 (33) (2021) eabh0638.

[14] A. Banerjee, T.M. Squires, Long-range, selective, on-demand suspension interactions: combining and triggering soluto-inertial beacons, Sci. Adv. 5 (8) (2019), eaax1893.

[15] Y. Long, C. Liu, B. Zhao, K. Song, G. Yang, C.-H. Tung, Bio-inspired controlled release through compression–relaxation cycles of microcapsules, NPG Asia Mater. 7 (1) (2015) e148.

[16] Q. Yan, R. Zhou, C. Fu, H. Zhang, Y. Yin, J. Yuan, Co2-responsive polymeric vesicles that breathe, Angew. Chem., Int. Ed. 50 (21) (2011) 4923–4927.

[17] F. Zhang, T. Zhao, D. Ruiz-Molina, Y. Liu, C. Roscini, J. Leng, S.K. Smoukov, Shape memory polyurethane microcapsules with active deformation, ACS Appl. Mater. Interfaces 12 (41) (2020) 47059–47064.

[18] D.M. Durieux, K.T. Du Clos, D.B. Lewis, B.J. Gemmell, Benthic jellyfish dominate water mixing in mangrove ecosystems, Proc. Natl. Acad. Sci. 118 (30) (2021) e2025715118.

[19] J. Song, F. Babayekhorasani, P.T. Spicer, Soft bacterial cellulose microcapsules with adaptable shapes, Biomacromolecules 20 (12) (2019) 4437–4446.

[20] M. Pepicelli, M.R. Binelli, A.R. Studart, P.A. Ruhs, P. Fischer, Self-grown bacterial cellulose capsules made through emulsion templating, ACS Biomater. Sci. Eng. 7 (7) (2021) 3221–3228.

[21] M. Hosseini, F. Babayekhorasani, Z. Guo, K. Liang, V. Chen, P.T. Spicer, Propulsion, deformation, and confinement response of hollow nanocellulose millimotors, J. Colloid Interface Sci. 628 (2022) 435–445.

[22] A. Halperin, M. Kröger, F.M. Winnik, Poly(N-isopropylacrylamide) phase diagrams: fifty years of research, Angew. Chem., Int. Ed. 54 (51) (2015) 15342–15367, https://doi.org/10.1002/anie.201506663.

[23] B.A. Humphreys, J.D. Willott, T.J. Murdoch, G.B. Webber, E.J. Wanless, Specific ion modulated thermoresponse of poly (n-isopropylacrylamide) brushes, Phys. Chem. Chem. Phys. 18 (8) (2016) 6037–6046.

[24] X. Sun, E. DenHartog, X. Zhang, M. McCord, Study of poly (n-isopropylacrylamide) grafted cotton fabrics initiated by atmospheric pressure plasma, Appl. Surf. Sci. 453 (2018) 182–191.

[25] E.M. Benetti, C. Kang, J. Mandal, M. Divandari, N.D. Spencer, Modulation of surface-initiated atrp by confinement: mechanism and applications, Macromolecules 50 (15) (2017) 5711–5718, https://doi.org/10.1021/acs.macromol.7b00919.

[26] W. Wu, J. Li, W. Zhu, Y. Jing, H. Dai, Thermo-responsive cellulose paper via arget atrp, Fiber Polym. 17 (4) (2016) 495–501.

[27] J. Lindqvist, D. Nyströḿ, E. Ostmark, P. Antoni, A. Carlmark, M. Johansson, A. Hult, E. Malmström, Intelligent dual-responsive cellulose surfaces via surface-initiated atrp, Biomacromolecules 9 (8) (2008) 2139–2145.

[28] H. Lönnberg, Q. Zhou, H. Brumer, T.T. Teeri, E. Malmström, A. Hult, Grafting of cellulose fibers with poly (ε-caprolactone) and poly (l-lactic acid) via ring-opening polymerization, Biomacromolecules 7 (7) (2006) 2178–2185.

[29] H. Kim, S.-M. Jo, F. Meng, Y. Guo, H. Thérien-Aubin, R. Golestanian, K. Landfester, E. Bodenschatz, One-step generation of core–gap–shell microcapsules for stimuli-responsive biomolecular sensing, Adv. Funct. Mater. 30 (50) (2020) 2006019.

[30] Y. Chen, W. Wei, Y. Zhu, J. Luo, R. Liu, X. Liu, Synthesis of temperature/ph dual-stimuli-response multicompartmental microcapsules via pickering emulsion for preprogrammable payload release, ACS Appl. Mater. Interfaces 12 (4) (2020) 4821–4832.

[31] F. Babayekhorasani, M. Hosseini, P.T. Spicer, Molecular and colloidal transport in bacterial cellulose hydrogels, Biomacromolecules 23 (6) (2022) 2404–2414.

[32] A.R. Rebelo, A.J. Archer, X. Chen, C. Liu, G. Yang, Y. Liu, Dehydration of bacterial cellulose and the water content effects on its viscoelastic and electrochemical properties, Sci. Technol. Adv. Mater. 19 (1) (2018) 203–211.

[33] G.W. Scherer, Theory of drying, J. Am. Ceram. Soc. 73 (1) (1990) 3–14.

[34] E.S. Ferreira, C.A. Rezende, E.D. Cranston, Fundamentals of cellulose lightweight materials: bio-based assemblies with tailored properties, Green Chem. (2021).

[35] S.J. Veen, A. Kuijk, P. Versluis, H. Husken, K.P. Velikov, Phase transitions in cellulose microfibril dispersions by high-energy mechanical deagglomeration, Langmuir (2014) 141028100140005.

[36] Y. Jin, T. Yang, S. Ju, H. Zhang, T.-Y. Choi, A. Neogi, Thermally tunable dynamic and static elastic properties of hydrogel due to volumetric phase transition, Polymers 12 (7) (2020) 1462.

[37] K.J. Tangso, H. Patel, S. Lindberg, P.G. Hartley, R. Knott, P.T. Spicer, B.J. Boyd, Controlling the mesostructure formation within the shell of novel cubic/hexagonal phase cetyltrimethylammonium bromide–poly (acrylamide-acrylic acid) capsules for ph stimulated release, ACS Appl. Mater. Interfaces 7 (44) (2015) 24501–24509.

[38] M. Zhang, Y. Li, Q. Yang, L. Huang, L. Chen, Y. Ni, H. Xiao, Temperature and ph responsive cellulose filament/poly (nipam-co-aac) hybrids as novel adsorbent towards pb (ii) removal, Carbohydr. Polym. 195 (2018) 495–504.

[39] J. Cui, M. Björnmalm, Y. Ju, F. Caruso, Nanoengineering of poly (ethylene glycol) particles for stealth and targeting, Langmuir 34 (37) (2018) 10817–10827.

[40] K. Katija, J.O. Dabiri, A viscosity-enhanced mechanism for biogenic ocean mixing, Nature 460 (7255) (2009) 624–626.

[41] W.H. Blackburn, L.A. Lyon, Size-controlled synthesis of monodisperse core/shell nanogels, Colloid Polym. Sci. 286 (5) (2008) 563–569, https://doi.org/10.1007/s00396-007-1805-7, https://www.ncbi.nlm.nih.gov/pmc/articles/PMC2528284.

[42] H. Kojima, F. Tanaka, C. Scherzinger, W. Richtering, Temperature dependent phase behavior of pnipam microgels in mixed water/methanol solvents, J. Polym. Sci., Part B, Polym. Phys. 51 (14) (2013) 1100–1111, https://doi.org/10.1002/polb.23194.

[43] J.M. Ottino, et al., Mixing, chaotic advection, and turbulence, Annu. Rev. Fluid Mech. 22 (1) (1990) 207–254.

[44] T.J. Murdoch, B.A. Humphreys, J.D. Willott, K.P. Gregory, S.W. Prescott, A. Nelson, E.J. Wanless, G.B. Webber, Specific anion effects on the internal structure of a poly(n-isopropylacrylamide) brush, Macromolecules 49 (16) (2016) 6050–6060, https://doi.org/10.1021/acs.macromol.6b01001.

[45] W.A. Braunecker, N.V. Tsarevsky, A. Gennaro, K. Matyjaszewski, Thermodynamic components of the atom transfer radical polymerization equilibrium: quantifying solvent effects, Macromolecules 42 (17) (2009) 6348–6360.

[46] J.L. Silverberg, A.R. Barrett, M. Das, P.B. Petersen, L.J. Bonassar, I. Cohen, Structure-function relations and rigidity percolation in the shear properties of articular cartilage, Biophys J. 107 (7) (2014) 1721–1730.

[47] D. Lee, D.A. Weitz, Double emulsion-templated nanoparticle colloidosomes with selective permeability, Adv. Mater. 20 (18) (2008) 3498–3503.

[48] C.A. Schneider, W.S. Rasband, K.W. Eliceiri, NIH image to ImageJ: 25 years of image analysis, Nat. Methods 9 (7) (2012) 671–675.

[49] T. Contributors, Trackpy, https://doi.org/10.5281/zenodo.4682814, http://soft-matter.github.io/trackpy/v0.5.0/index.html.

[50] T.G. Mason, J. Bibette, D.A. Weitz, Elasticity of compressed emulsions, Phys. Rev. Lett. 75 (10) (1995) 2051–2054.